New Results on the Omega-K Algorithm for Processing Synthetic Aperture Radar Data

Matthew A. Tolman and David G. Long
Electrical and Computer Engineering Dept.
Brigham Young University, 459 CB, Provo, Utah 84602
Email: long@ee.byu.edu

***Abstract*— This paper compares the peak SNR and the point target impulse response function of stripmap SAR data processed with the well-known Omega-k algorithm and ideal matched filtering. The impulse response function resulting from Omega-k is distorted and stretched in azimuth compared to a matched filter. The distortion depends on the amount of frequency shift required in the Stolt mapping step. In at least some cases, the range resolution is improved compared to matched filtering at the expanse of additional azimuth interference.**

I. Introduction

The so-called Omega-k algorithm is commonly used for processing raw stripmap synthetic aperture radar (SAR) data into backscatter images. While the algorithm is well-known [1], [2], [3], [4], a number of its features are not fully recognized. In this paper we explore a number of aspects of the algorithm, including the peak signal-to-noise ratio (SNR) and the behavior of the point-spread function. For example, the Omega-k algorithm does not achieve the same SNR as an optimum matched filter.

It is shown that the focused point spread function obtained with the Omega-k algorithm differs from the output of a matched filter. Compared to optimal time-domain processing, the sidelobes and mainlobe of the point target response are stretched by the Omega-k algorithm. However, the amplitude of the Omega-k sidelobes is somewhat lower than that observed for the optimum matched filter. The impact of these observations on potential interference with nearby scatterers is considered. We propose a modification of the algorithm which enables it to achieve optimum peak SNR.

II. Background

Figure 1 illustrates the geometry for stripmap SAR. We consider only straight-line motion and broadside imaging. With this geometry, it can be shown that the range-compressed, time-domain SAR signal for a point target at (x_0, y_0, z_0) with a slant range of closet approach (SRCA) r at an azimuth of z_0, can be expressed exclusively in terms of the spatial variables ρ (slant range) and z (azimuth displacement) as [5]

$$\begin{aligned} v(\rho, z) &= \frac{C}{\left[r^2 + (z - z_0)^2\right]^2} A\left(\frac{z - z_0}{r}\right) \cdot \\ &\quad h_\rho\left(\rho - \sqrt{r^2 + (z - z_0)^2}\right) \cdot \\ &\quad e^{-j2\pi f_{\rho 0}\sqrt{r^2 + (z - z_0)^2}} e^{j\phi_{target}}, \end{aligned} \tag{1}$$

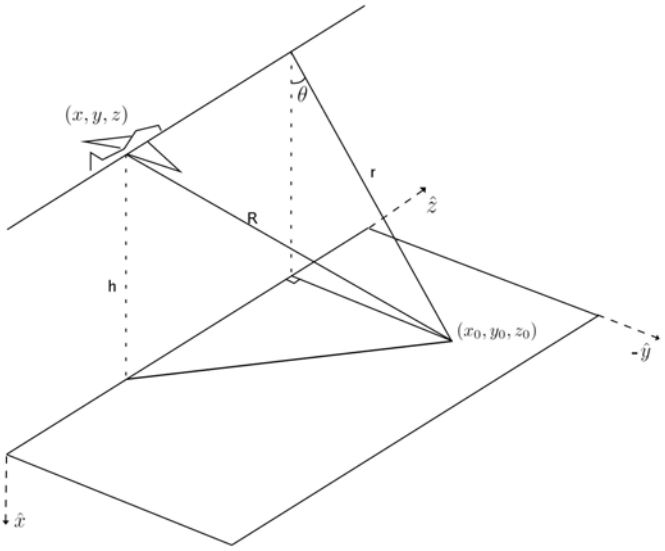

Fig. 1. An illustration of the three dimensional geometry for stripmap SAR sensors. The slant range of closest approach is denoted r.

where C is a constant which includes the transmit power, the target's radar cross-section, the radar wavelength, and the $1/(4\pi)^3$ term; $A(\cdot)$ is two-way antenna gain; $h_\rho(\cdot)$ is the net effective system range filter response function (including range chirping); $f_{\rho 0} = 2f_0/c$ is constant defined as twice the radar carrier frequency f_0 in cycles per meter; and ϕ_{target} is the target phase.

Taking the two-dimensional Fourier transform in slant range and azimuth of Eq. 1 using the principle of stationary phase (POSP), the signal in the spatial frequency domain is [5]

$$\begin{aligned} V(f_\rho, f_z) &= C \frac{\left[(f_\rho + f_{\rho 0})^2 - f_z^2\right]^{\frac{5}{4}}}{r^{\frac{7}{4}}(f_\rho + f_{\rho 0})^3} \cdot \\ &\quad A\left(\frac{f_z}{\sqrt{(f_\rho + f_{\rho 0})^2 - f_z^2}}\right) H_\rho(f_\rho) \cdot \\ &\quad e^{-j\frac{\pi}{4}} e^{j\phi_{target}} e^{-j2\pi r\sqrt{(f_\rho + f_{\rho 0})^2 - f_z^2} - j2\pi f_z z_0}. \end{aligned} \tag{2}$$

where f_ρ is range frequency, f_z is azimuth frequency, and $H_\rho(f_\rho)$ is the Fourier transform of $h_\rho(\rho)$. The first exponential corresponds to a delay term.

The frequency domain support of the SAR signal is entirely

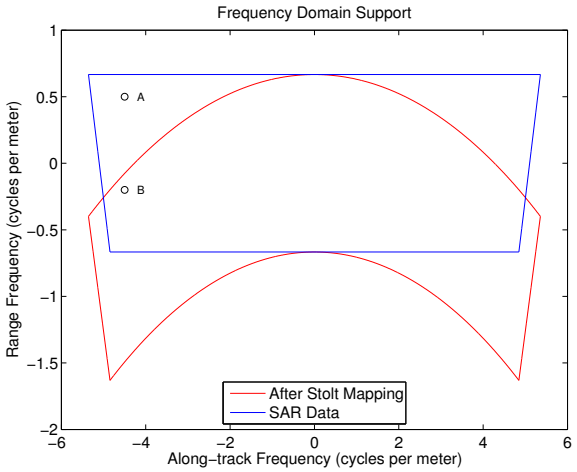

Fig. 2. Comparison of the frequency domain support of the SAR signal before (blue trapezoid) and after (red curvilinear shape) the Stolt mapping, illustrated for the case of an L-band SAR system with a 60 degree beamwidth and a 500MHz range chirp. Note that due to the Stolt mapping, the effect of the Omega-k algorithm is to move energy in the range frequency direction from one location in the frequency domain to another, i.e. moving point A to point B.

determined by $H_\rho(f_\rho)$ and the antenna gain $A(\cdot)$. The range frequency filtering function $H_\rho(f_\rho)$ is a function only of range frequency, and limits the support of the function in that dimension. The antenna weighting function limits the azimuth frequencies; however, we note that such limits depend on the range frequency as well as the azimuth frequency. Figure 2 illustrates the 3 dB spatial frequency domain support of the SAR signal.

A. The Omega-K Algorithm

The Omega-k algorithm was first applied to SAR by [1]. An alternate signal processing development of the algorithm is presented in [3]. While the details vary between implementations, the Omega-k algorithm requires a change of variables in the frequency domain referred to as Stolt mapping [6]. This mapping reduces the phase variation in the frequency domain to phase ramps which center the signal around its azimuth position and the SRCA of the target, a result very similar to that of the matched filter.

From the last term in Eq. 2, the relevant portion[1] of the frequency domain phase is

$$\theta_{2dfft} = -2\pi r\sqrt{(f_\rho + f_{\rho 0})^2 - f_z^2} - 2\pi f_z z_0 \qquad (3)$$

and consists of two terms. The last term in Eq. 3 is the linear ramp desired to center the signal on the azimuth position of the target. While the first term is a function of the target's SRCA, it is not a linear phase term and cannot be altered using phase multiplies because the SRCA r for the target is unknown. This term is changed into a linear phase ramp by a change of variables according to

$$\sqrt{(f_\rho + f_{\rho 0})^2 - f_z^2} = \tilde{f}_\rho + f_{\rho 0}, \qquad (4)$$

which is the Stolt mapping, a 1-dimensional process (see Fig. 2). The signal is mapped from frequencies f_ρ to $\tilde{f}_\rho$ where the mapping depends on the value of f_z. Performing the change of variables according to Eq. 4 reduces the frequency domain phase to

$$\begin{aligned}\theta_{2dfft} &= -2\pi r(\tilde{f}_\rho + f_{\rho 0}) - 2\pi f_z z_0 \\ &= -\underbrace{2\pi \tilde{f}_\rho r}_{\text{SRCA Delay}} - \underbrace{2\pi f_z z_0}_{\text{Azimuth Delay}} - \underbrace{2\pi f_{\rho 0} r}_{\text{Carrier Phase}}, \end{aligned} \qquad (5)$$

where the first term is a shift in the range direction, the second is a shift in the azimuth direction, and the last is a constant phase term associated with the SRCA. Often ignored, the last term is of interest for interferometric SAR.

The Omega-k algorithm is an interesting approach to the problem of focusing the raw SAR data. In the frequency domain a matched filter cannot be applied because the signal is range dependent. Instead, the Omega-k algorithm moves the frequency domain signal to a new position in the frequency domain as illustrated in Fig. 2 where the phase is appropriate for forming an image (focusing the target) using the inverse Fourier transform. Even though the phase modulation in the frequency domain depends on the target's SRCA, the frequency domain mapping necessary to focus the data is the same regardless of the target's SRCA. The Omega-k algorithm exploits this relationship to focus the SAR data.

III. Algorithm Analysis

While the Omega-k is not an exact matched filter, with a simple modification, the Omega-k algorithm achieves a SNR that, aside from possible POSP approximation errors, is the same as that achieved by a matched filter. Note that while a matched filter achieves compression by frequency domain multiplication, the Omega-k algorithm avoids this by moving the frequency domain signal from one location in the frequency domain to another via the Stolt mapping. This difference in approach has an effect on the focused impulse response as explored in the following.

A. Peak SNR

In the space domain, the ideal matched filtered signal corresponding to a point target at (r, z_0) can be computed from the frequency domain signal given in Eq. 2. The frequency domain signal is factored into constant target-dependent components, linear frequency ramps in range and azimuth, the range frequency response, and other spatial frequency-dependent response terms. The matched filter frequency response corresponds to the complex conjugate of the latter. Applying this

[1]There are additional phase terms in Eq. 2, but they are constant or are associated with the antenna pattern. Antenna phase terms are not compensated for by the Omega-k algorithm.

matched filter frequency response to Eq. 2 yields,

$$V(f_\rho, f_z) = \left| \frac{((f_\rho + f_{\rho 0})^2 - f_z^2)^{\frac{5}{4}}}{r^{\frac{7}{4}}(f_\rho + f_{\rho 0})^3} \cdot A\left(\frac{f_z}{\sqrt{(f_\rho + f_{\rho 0})^2 - f_z^2}}\right)\right|^2 H_\rho(f_\rho) \cdot k e^{-j\frac{\pi}{4}} e^{j\phi_{target}} \cdot e^{-j2\pi f_\rho r - j2\pi f_{\rho 0} r - j2\pi f_z z_0}, \quad (6)$$

where the bottom terms are the phase ramps and constant and target terms. This is the frequency response of a point target.

Evaluating the inverse Fourier transform at the position of the target (r, z_0) yields

$$v(r, z_0) = \frac{k}{r^{\frac{7}{4}}} e^{-j\frac{\pi}{4}} e^{j\phi_{target}} e^{-j2\pi f_{\rho 0} r} \int_{-\infty}^{\infty}\int_{-\infty}^{\infty} H_\rho(f_\rho) \left|\frac{((f_\rho + f_{\rho 0})^2 - f_z^2)^{\frac{5}{4}}}{(f_\rho + f_{\rho 0})^3} A\left(\frac{f_z}{\sqrt{(f_\rho + f_{\rho 0})^2 - f_z^2}}\right)\right|^2 df_\rho df_z, \quad (7)$$

which is the ideal matched filter complex image pixel value for the target. Note that the linear phase ramps in Eq. 6 are canceled by the exponentials of the inverse Fourier transform.

In contrast, to compute the Omega-k output at the pixel, the Stolt mapping is applied to the frequency domain represenation in Eq. 2. Then, the inverse Fourier transform is computed and evaluated at the target location. After Stolt mapping is applied, Eq. 2 becomes [5]

$$V(\tilde{f}_\rho, f_z) = k\frac{(\tilde{f}_\rho + f_{\rho 0})^{\frac{5}{2}}}{r^{\frac{7}{4}}((\tilde{f}_\rho + f_{\rho 0})^2 + f_z^2)^{\frac{3}{2}}} \cdot H_\rho\left(\sqrt{(\tilde{f}_\rho + f_{\rho 0})^2 + f_z^2} - f_{\rho 0}\right) \cdot A\left(\frac{f_z}{\tilde{f}_\rho + f_{\rho 0}}\right) e^{-j\frac{\pi}{4}} e^{j\phi_{target}} \cdot e^{-j2\pi \tilde{f}_\rho r - j2\pi f_{\rho 0} r - j2\pi f_z z_0}. \quad (8)$$

The inverse Fourier transform (focused image) evaluated at the target location (r, z_0) can be expressed as

$$v(r, z_0) = \frac{k}{r^{\frac{7}{4}}} e^{-j\frac{\pi}{4}} e^{j\phi_{target}} e^{-2\pi f_{\rho 0} r} \cdot \int_{-\infty}^{\infty}\int_{-\infty}^{\infty} H_\rho\left(\sqrt{(\tilde{f}_\rho + f_{\rho 0})^2 - f_z^2} - f_{\rho 0}\right) \cdot A\left(\frac{f_z}{\tilde{f}_\rho + f_{\rho 0}}\right) \frac{(\tilde{f}_\rho + f_{\rho 0})^{\frac{5}{2}}}{((\tilde{f}_\rho + f_{\rho 0})^2 + f_z^2)^{\frac{3}{2}}} \cdot \frac{|\tilde{f}_\rho + f_{\rho_0}|}{\sqrt{(\tilde{f}_\rho + f_{\rho 0})^2 + f_z^2}} d\tilde{f}_\rho df_z, \quad (9)$$

where the last line contains the Jacobian term for the change of variables, and the linear phase ramps in Eq. 8 are canceled by the exponentials of the inverse Fourier transform.

To simplify comparison with the matched filter output, the Stolt mapping is reversed to yield

$$v(r, z_0) = \frac{k}{r^{\frac{7}{4}}} e^{-j\frac{\pi}{4}} e^{j\phi_{target}} e^{-2\pi f_{\rho 0} r} \cdot \int_{-\infty}^{\infty}\int_{-\infty}^{\infty} H_\rho(f_\rho) A\left(\frac{f_z}{\sqrt{(f_\rho + f_{\rho 0})^2 - f_z^2}}\right) \cdot \frac{((f_\rho + f_{\rho 0})^2 - f_z^2)^{\frac{5}{4}}}{(f_\rho + f_{\rho 0})^3} df_\rho df_z. \quad (10)$$

The key differences between the matched filter (Eq. 7) and Omega-k (Eq. 10) algorithms occur in the integral. Using the known antenna azimuth gain pattern, the integrand in the Omega-k result can be multiplied by

$$A^*\left(\frac{f_z}{\sqrt{(f_\rho + f_{\rho 0})^2 - f_z^2}}\right) \frac{((f_\rho + f_{\rho 0})^2 - f_z^2)^{\frac{5}{4}}}{(f_\rho + f_{\rho 0})^3} \quad (11)$$

to yield the same result as the matched filter. Thus, the modification of the Omega-k algorithm by multiplying the Stolt interpolated signal by Eq. 11 achieves the same peak signal power as the matched filter, within the limitations of the errors in the POSP approximation used to derive the azimuth Fourier transform. Fortunately, this not generally a significant limitation and the achieved peak signal power is valid for targets appearing at all SRCA values.

B. Stolt Mapping

While the modified Omega-k algorithm achieves an SNR similar to that of the ideal matched filter, the spatial response functions are not the same since, as previously noted, the matched filter uses frequency domain multiplication, while the Omega-k algorithm moves energy around in the frequency domain via Stolt mapping. Here we explore the differences between the two resulting point spread functions.

In the following, the effects of different design choices on the magnitude of the Stolt mapping are evaluated in two steps: first, the values of f_z and f_ρ which result in the largest shift are identified; then, the effect of the azimuth bandwidth and the radar carrier frequency is developed. As previously noted, the Stolt mapping shifts energy from the original range frequency f_ρ to the new range frequency $\tilde{f}_\rho$ according to

$$\tilde{f}_\rho = \sqrt{(f_{\rho 0} + f_\rho)^2 - f_z^2} - f_{\rho 0}. \quad (12)$$

When $f_z = 0$, $\tilde{f}_\rho$ is equal to f_ρ. For other values of f_z, $\tilde{f}_\rho$ is less than f_ρ. While the difference between them is greatest for the maximum value of f_z, that maximum value of f_z varies for different values of f_ρ. Note that $f_{z,max} = (f_\rho + f_{\rho 0})\sin(\phi_{max})$ where ϕ_{max} is the maximum angle at which the target is seen by the antenna[2]. Using this value for f_z in Eq. 12 yields

$$\tilde{f}_\rho = \sqrt{(f_\rho + f_{\rho 0})^2 - (f_\rho + f_{\rho 0})^2 \sin^2(\phi_{max})} - f_{\rho 0} = (f_\rho + f_{\rho 0})\cos(\phi_{max}) - f_{\rho 0}, \quad (13)$$

[2]The exact choice of maximum is not critical for the discussion.

so the difference between f_ρ and $\tilde{f}_\rho$ is

$$f_\rho - \tilde{f}_\rho \quad = \quad (f_\rho + f_{\rho 0})(1 - \cos(\phi_{max})). \qquad (14)$$

For a fixed maximum angle, the magnitude of the Stolt shift is greatest for the largest value of f_ρ. Thus, the Stolt mapping which corresponds to the largest frequency domain shift is

$$\tilde{f}_{\rho,max} = \sqrt{(f_{\rho,max} + f_{\rho 0})^2 - f_{z,max}^2} - f_{\rho 0}, \qquad (15)$$

where $f_{\rho,max}$ is the maximum range frequency, and $f_{z,max}$ is the corresponding maximum azimuth frequency.

Following the idea of the Q of a filter, which is the ratio of the filter bandwidth to the center frequency, we define the Omega-k Q as the the ratio of the magnitude of the Stolt shift to the range bandwidth,

$$\begin{aligned} Q \quad &= \quad \frac{f_{\rho,max} - \tilde{f}_{\rho,max}}{f_{\rho,max}} \quad = \quad \left(1 - \frac{\tilde{f}_{\rho,max}}{f_{\rho,max}}\right) \qquad (16) \\ &= \quad 1 - 2\sqrt{\left(\frac{1}{2} + \frac{f_{\rho 0}}{2f_{\rho,max}}\right)^2 - \left(\frac{f_{z,max}}{2f_{\rho,max}}\right)^2} + \frac{f_{\rho 0}}{f_{\rho,max}}, \end{aligned}$$

where an increase in the value of Q is associated with a more significant shift. Note that the actual values of azimuth bandwidth and radar carrier frequency are not important. Instead, it is their value relative to the range bandwidth.

The maximum azimuth frequency $f_{z,max}$ appears in Q only under the radical term, and increasing the ratio of the maximum azimuth frequency to the range bandwidth increases the value of Q. The radar carrier frequency, on the other hand, appears in two terms which have opposite effects on Q. The net effect of increasing the radar carrier frequency to range bandwidth ratio is a decrease in the relative magnitude of the Stolt shift. This is illustrated in Fig. 3.

In summary, the significance of the Stolt mapping is related to two ratios: the ratio of the carrier frequency to the range bandwidth, and the ratio of the azimuth bandwidth to the range bandwidth. For the purposes of comparing two systems, the ratio of the azimuth bandwidth to the range bandwidth is effectively the ratio of the azimuth resolution to the range resolution. This ratio is greater than one for systems with an azimuth resolution which is higher than the range resolution. While the total effect of the Stolt mapping depends on many aspects of the SAR signal (the time-bandwidth product of the range chirp, the actual antenna pattern, etc.), comparing these ratios provides a reasonable starting point for analyzing the significance of the frequency domain shift.

C. Algorithm Performance Comparison

To illustrate the net effect of Stolt mapping for different bandwidth ratios, we compare the matched filter and Omega-k impulse responses computed for two cases. The first case SAR signal has a 500 MHz carrier, a 200 MHz range bandwidth, and a 45° beamwidth. The carrier to range bandwidth ratio is 2.5, while the azimuth resolution is roughly twice the range resolution. The second case SAR signal has a 2 GHz carrier, a 200 MHz range chirp, and a 45° beamwidth. The carrier

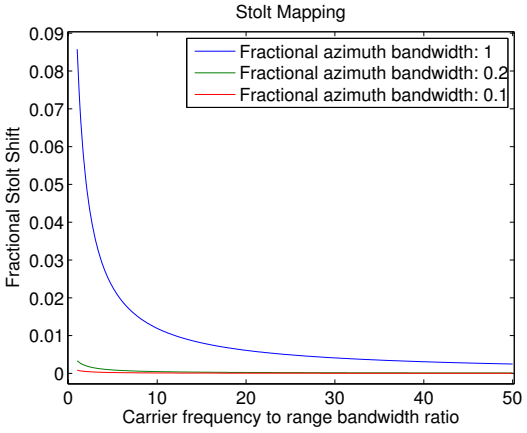

(a) Low bandwidth ratios

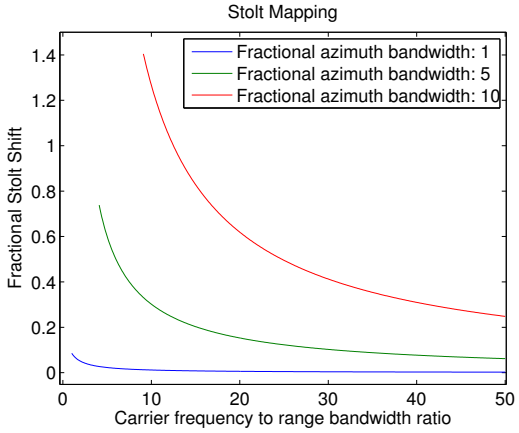

(b) High bandwidth ratios

Fig. 3. Plots of the ratio of the largest frequency domain shift to the range bandwidth for various azimuth to range bandwidth ratios. The fractional azimuth bandwidth is defined as $f_{z,max}/f_{\rho,max}$, and the fractional Stolt shift is given by Eq. 16. The frequency domain shift becomes more significant as the radar carrier decreases and the azimuth bandwidth increases (see text).

to range bandwidth ratio is ten, and the azimuth resolution is about ten times greater than the range resolution. Note that while the antenna azimuth beamwidth is the same for both systems, the azimuth bandwidth is greater for case two due to the higher carrier frequency. Figure 4 illustrates the regions of support in the frequency domain for each case. Note that significantly more frequency movement in the Stolt mapping is required at extreme azimuth frequencies for case two.

The ideal point target impulse responses for each case are shown in Fig. 5. For both cases, the simulated data is processed by the Omega-k algorithm, and the residual frequency domain phase of the signal is removed. The resulting point spread function is compared to the output of a modified version of the matched filter (MF) which is obtained by canceling out

the frequency domain phase of the raw SAR signal.

Note that in case two, where more frequency shift is done in the Stolt mapping, the sidelobes are more distorted, which could impact target interference. Note, however, that when we examine the mainlobe (see Fig. 6) a surprising result is observed for case two. Typically, the 3dB contour of the point spread function defines the system resolution. For case two, the 3dB contour is compressed in range into more of a rectangular shape as shown in Fig. 6. While the 3dB width in azimuth is largely unaffected by the Stolt mapping, the 3dB width in range is reduced by about factor of two. Thus, the increased azimuth bandwidth results in improved range resolution. The improvement does not come without cost. While the 3dB contour can be improved in one direction (i.e., slant range), the main lobe is stretched in the other direction (i.e., in azimuth). As a result, more interference is expected for targets which are closely spaced diagonally or closely spaced in azimuth for data processed with Omega-k than for the ideal matched filter case.

IV. Conclusion

The Omega-k algorithm, with modification, can achieve the same peak SNR as an ideal matched filter. However, the frequency domain shift (Stolt mapping) used by the Omega-k algorithm to focus the data alters the point target impulse response function. The differences decrease the potential interference between targets separated in range but increase the potential interference between targets separated in azimuth or diagonally. In addition, the Stolt mapping introduces a phase modulation across the main lobe which may affect the accuracy of interferometric SAR systems.

References

[1] C. Cafforio, C. Prati, and F. Rocca, "SAR data focusing using seismic migration techniques," *IEEE Transactions on Aerospace and Electronic Systems*, vol. 27, no. 2, pp. 194–207, 1991.

[2] R. Bamler, "A comparison of range-doppler and wavenumber domain SAR focusing algorithms," *IEEE Transactions on Geoscience and Remote Sensing*, vol. 30, no. 4, pp. 706–713, Jul 1992.

[3] I. G. Cumming and F. H. Wong, *Digital Processing of Synthetic Aperture Radar Data*, Artech House, 2005.

[4] I. Cumming, Y. Neo, and F. Wong, "Interpretations of the Omega-k algorithm and comparisons with other algorithms," *Proceedings 2003 IEEE International Geoscience and Remote Sensing Symposium*, vol. 3, pp. 1455–1458, July 2003.

[5] M. A. Tolman, *A Detailed Look at the Omega-K Algorithm for Processing Synthetic Aperture Radar Data*, Master's Thesis, Brigham Young University, Dec. 2008.

[6] R. H. Stolt, "Migration by Fourier transform," *Geophysics*, vol. 43, no. 1, pp. 23–48, 1978.

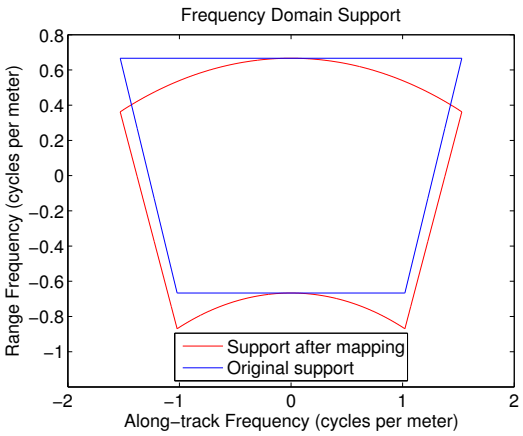

(a) Case one

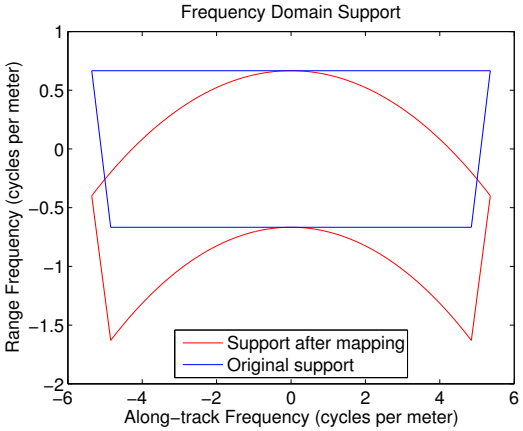

(b) Case two

Fig. 4. An illustration of the frequency domain support of the two simulated SAR signals before and after the Stolt mapping (see text). Case one is a SAR system with a large range bandwidth compared to the radar carrier frequency. Case two is a SAR system with a large azimuth bandwidth to emphasize the effect of the Stolt mapping.

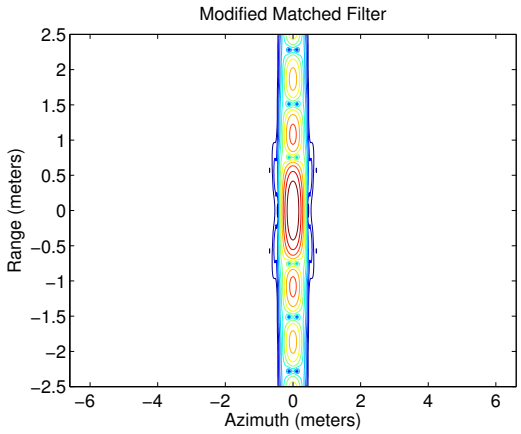

(a) MF, Case one

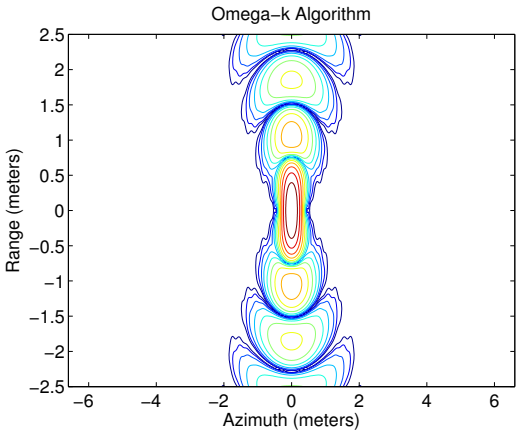

(b) Omega-k, Case one

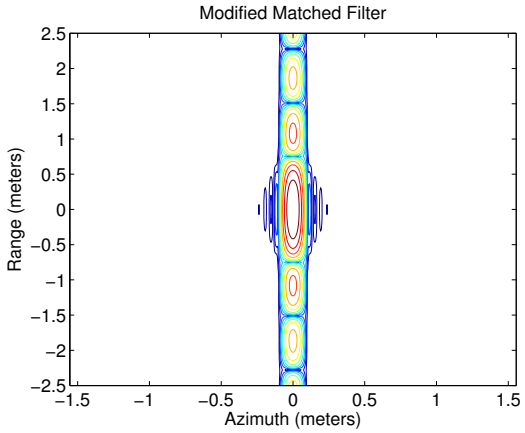

(c) MF, Case two

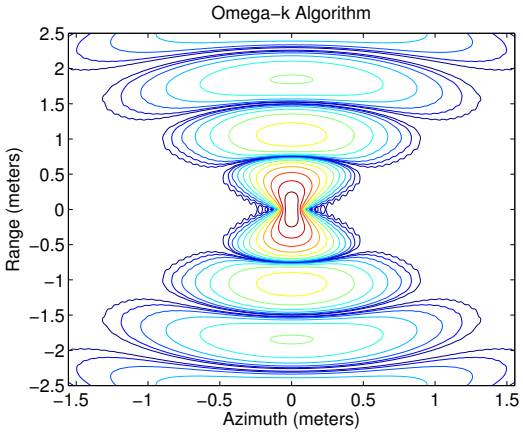

(d) Omega-k, Case two

Fig. 5. Contour plots of the focused SAR signal for each case for an ideal point target with contours from -5dB to -55dB at 5dB intervals for the (left column) modified matched filter (MF) and (right column) Omega-k processing algorithms. A zoom-in of the central peak for case two is shown in Fig. 6.

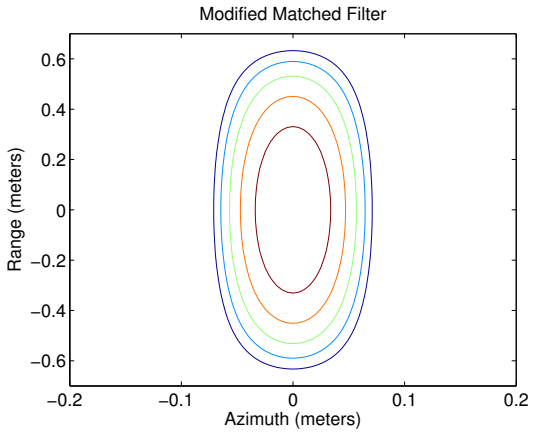

(a) Modified Matched Filter

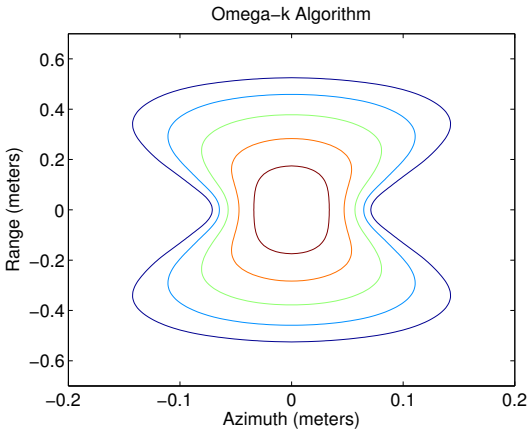

(b) Omega-k Algorithm

Fig. 6. Close up contour plots of the main lobe for case two in Fig. 5 with contours from -3dB to -15dB at 3dB intervals. While the main lobe is quite distorted by the Stolt mapping, the 3db contour (the innermost contour) is smaller for Omega-k, resulting in improved range resolution. This improvement comes at the cost of increased interference between scatterers separated in azimuth or separated diagonally.